

**Evolution of fumarolic anhydrous copper sulfate minerals during successive
hydration/dehydration**

Oleg I. Siidra, ^{*,1} Artem S. Borisov,¹ Dmitri O. Charkin,²

Wulf Depmeier,³ Natalia V. Platonova⁴

¹ *Department of Crystallography, St. Petersburg State University, University Embankment 7/9,
199034 St. Petersburg, Russia*

² *Chemistry Department, Moscow State University, Leninskie Gory 1-3, Moscow 199992 Russia*

³ *Institut für Geowissenschaften der Universität Kiel, Olshausenstr. 40, D-24098 Kiel, Germany*

⁴ *X-ray Diffraction Resource Center, St. Petersburg State University, University Embankment
7/9, 199034 St. Petersburg, Russia*

* E-mail: o.siidra@spbu.ru

Abstract

Hydration processes of primary anhydrous minerals as well as dehydration of the hydrated phases are relevant not only for answering geochemical and petrological questions, but are also interesting in the context of the theory of «Evolution of minerals». Our study of the evolution of anhydrous exhalative sulfates in hydration and dehydration processes has demonstrated the complexity of the processes for a number of minerals from the active high-temperature fumaroles of Tolbachik volcano (chalcocyanite $\text{Cu}(\text{SO}_4)$, dolerophanite $\text{Cu}_2\text{O}(\text{SO}_4)$, alumoklyuchevskite $\text{K}_3\text{Cu}_3\text{AlO}_2(\text{SO}_4)_4$, and itelmenite $\text{Na}_2\text{CuMg}_2(\text{SO}_4)_4$). The hydration and dehydration experiments with all four studied minerals were carried out using PXRD. A typical structural characteristic of several anhydrous copper sulfate minerals of fumarolic origin is the presence of oxygen-centered OCu_4 tetrahedra. These are absent in the structures of all known hydrated minerals or synthetic compounds of the class under consideration. Hydration of minerals initially containing O^{2-} anions as part of oxocomplexes, proceeds with sequential formation of a large series of hydroxysalts. On

the contrary, hydration of itelmenite with its relatively complex “initial” structure, but without additional oxygen atoms, which are strong Lewis bases, results in formation of simpler hydrates. The lower the temperature and the larger the excess of water, the stronger the tendency of the cations to adopt higher hydration numbers thus outcompeting the sulfate anions as ligands. Ultimately, the water molecules completely expel the bridging sulfate anions from the metal coordination sphere yielding relatively simple fully hydrated structures.

Keywords: evolution of minerals; sulfates; reversible hydration/dehydration; fumarolic minerals; X-ray diffraction.

Introduction

Hydration processes of primary anhydrous minerals as well as dehydration of the hydrated phases are relevant not only for answering geochemical and petrological questions, but can also claim interest in the context of the theory of «Evolution of minerals» (Hazen et al., 2008). One important piece of this theory refers to the observation that new mineral species formed by hydration are usually more complex than the pristine ones and often more than one secondary species are formed from a given primary mineral. There are many more important aspects of hydration/oxidation processes, e.g. their role in the formation of economic mineral deposits or their possible ecological threat as these processes are often the first steps of destructive weathering and thereby possible release of toxic elements into the environment with all kind of subsequent detrimental effects.

In the past few decades, hydration and dehydration processes of sulfate minerals, especially those containing iron, have been studied (Sklute et al., 2018; Xu et al., 2009). Much systematic work has been devoted to the study of hydration and dehydration processes in the magnesium - sulfate - water system, in view of understanding the paleo-atmospheric conditions on Mars (e.g. Vaniman et al., 2004; Chipera and Vaniman, 2007; Altheide et al., 2009; Grevel and Majzlan, 2009). Note that all of the cited publications - and other ones not cited here for lack of space - concern primarily simple systems such as $\text{Fe}(\text{SO}_4) - \text{H}_2(\text{SO}_4) - \text{H}_2\text{O}$ or $\text{Mg}(\text{SO}_4) - \text{H}_2(\text{SO}_4) - \text{H}_2\text{O}$. Systems containing other cations, e.g. other transition metals instead of Fe, or additional main group cations such as Na or K, or anions like halides, have received less attention to date.

Anhydrous high-temperature sulfate minerals with transition metals such as iron, copper, zinc, vanadium *etc.* are quite exotic mineral species, and occur almost exclusively in fumaroles of

active volcanoes - in a few cases they also form by natural underground coal fires (e.g. Pautov et al., 2020). Often these minerals become unstable under changing temperature conditions and especially when they are exposed to humid atmosphere or to precipitation. When this happens they may rapidly hydrate and undergo various chemical and physical transformations, including repeated dissolution - crystallization cycles. Re-heating by exhausting hot gases from the fumarole may lead to dehydration with either recovery of the pristine minerals, or crystallization of new species. The chemical compositions as well as the structural architectures of many fumarolic minerals are unique and have no analogs among synthetic compounds, which makes them also interesting for inorganic crystal chemistry and materials science. Likewise of interest is the possible occurrence of metastable transient phases upon hydration or dehydration, which are often inaccessible via traditional synthetic routes.

Fumaroles on active volcanoes can be subdivided into two groups: i) fumaroles with oxidizing conditions and ii) fumaroles with reducing mineral formation environments. The latter are much more common and have been well studied in terms of mineralogy; common primary mineral species are native elements, sulfides and sulfosalts, overall, the mineral inventory is relatively poor and uniform. In stark contrast to the latter, oxidizing fumaroles are much less common on Earth and they differ significantly in the number and variety of mineral species. Some of the best-studied fumaroles with oxidizing conditions are located at the Vesuvius volcano where they show remarkable copper oxide mineralization (Balassone et al., 2019). The Vesuvius fumaroles have been known since antiquity. In the middle of the 20th century, oxidizing fumaroles of the Izalco volcano in Salvador came under study and revealed a rich anhydrous copper-vanadium mineralization (Hughes and Stoiber, 1985). Half a century ago, in 1975-1976, one of the most famous eruptions of the 20th century rocked the Tolbachik volcano located on the Kamchatka Peninsula, Russian Federation. This became known as the Great Fissure Tolbachik Eruption (GFTE) (Fedotov and Markhinin, 1983). Several scoria cones were formed and the associated fumaroles turned out to be real bonanzas providing amazingly rich and diverse mineral associations which have become a veritable playground for the study of the mineralogy and crystal chemistry of volcanic exhalations (Vergasova and Filatov, 2012, 2016; Pekov et al., 2018 a,b). In 2012, another important eruption occurred on the Tolbachik volcano - the Fissure Tolbachik Eruption (FTE). The copper mineralization in the fumaroles of the Second Scoria Cone of GFTE was so rich that at the end of the 70s of the last century these fumaroles were valued as a very rich though small copper deposit and a possible mining was taken into consideration. Fortunately, this idea was dropped because the remoteness and inaccessibility of this deposit made its possible exploitation uneconomic. The fumaroles became world-renowned, not so much as a reservoir of copper, but rather for the high number of different endemic mineral species, as well as for the total

mineral diversity, which makes it second to none on our planet, at least to this date. Note that the areas holding productive fumaroles are rather small: the fumarole field on the Second Scoria Cone for example extends over just a few hundred square meters. Nevertheless, more than 110 new mineral species have been described from the fumaroles of GFTE and FTE until this date. We also contributed to this list by the discovery and study of a number of new anhydrous sulfate mineral species from the fumaroles of both localities (Siidra et al., 2014a, 2017, 2018a, b, c, 2019b, c, 2020a, b; Nazarchuk et al., 2018, 2020). It is most likely that the list of new minerals discovered in the fumaroles of the Tolbachik volcano is far from being complete. Post-eruptive processes are still going on and formation of new mineral species is observed. The temperature in the fumaroles is by no means constant but changes over time, whereby the changes may happen in either directions, rising or falling. Some of the fumaroles which were active decades ago, are now extinct. As a result of alteration by hydration processes, the formation of unique associations of secondary hydrated sulfate minerals is observed (e.g. Siidra et al., 2014b, c). However, the transformation of primary fumarolic minerals under the influence of atmospheric moisture is only poorly studied to date. The temperature regime in the upper fumarole zones is subject to seasonal fluctuations due to the large amount of atmospheric precipitations. The first systematic studies of these processes were carried out by our group (Siidra et al., 2019a) on the example of euchlorine $\text{KNaCu}_3\text{O}(\text{SO}_4)_3$ and they demonstrated an unexpected complexity of such processes, both in the number of phases formed and in the transformations of multiphase aggregates as a function of changing temperatures. The current paper expands these studies to cover a larger set of fumarolic minerals.

The Yadovitaya (Russian for Poisonous) fumarole is located in the fumarole field on the summit of the Second Scoria Cone of the Northern Breakthrough of the GFTE. The field is located approximately 18 km SSW from the active shield volcano Ploskiy (flat) Tolbachik (Fedotov and Markhinin, 1983). The Yadovitaya fumarole was one of the first fumaroles described after the GFTE (Vergasova and Filatov, 2016). The intensity of the gas streams in this fumarole varied greatly in the first years after the eruption (Menyailov et al., 1980) and Yadovitaya fumarole is still very active to date. The diversity in the number of endemic copper sulfate mineral species with various additional cations and anions in the Yadovitaya fumarole is impressive. Figure 1a shows a photograph of the freshly cleared fumarole wall to a depth of 2.5 meters as of September 2019. The Cu-SO₄ zone enriched in various anhydrous copper sulfates ranges from 35 cm to 65-70 cm below the top of the fumarole, it is marked by red lines on Fig. 1a. All the mineral samples (Figure 1b,d,e) used for hydration experiments described below were collected from this zone. The temperature of exhausting gases registered on the level of the Cu-SO₄ zone was approximately 300°C. All the recovered samples were packed and isolated immediately after collection in order to protect them from contact with the external atmosphere. Chalcocyanite, dolerophanite and

alumoklyuchevskite were obviously deposited directly as sublimates from volcanic gas emissions, whereas the origin of itelmenite, which contains a significant amount of Mg, is supposed to be the product of a reaction between volcanic gases and the basaltic scoria. This is corroborated by the fact that possible relevant Mg compounds have very low volatility at 300°C, hence direct sublimation of this mineral is deemed improbable. On the top of the fumarole, on the outcrop, there is a zone (~ 10 cm) with variable fluoride mineralization. Between the fluoride zone and the Cu-SO₄ zone, a 15 to 25 cm thick intermediate zone composed of altered and hydrated copper-sulfate minerals is easily discerned by its coloration (Fig. 1).

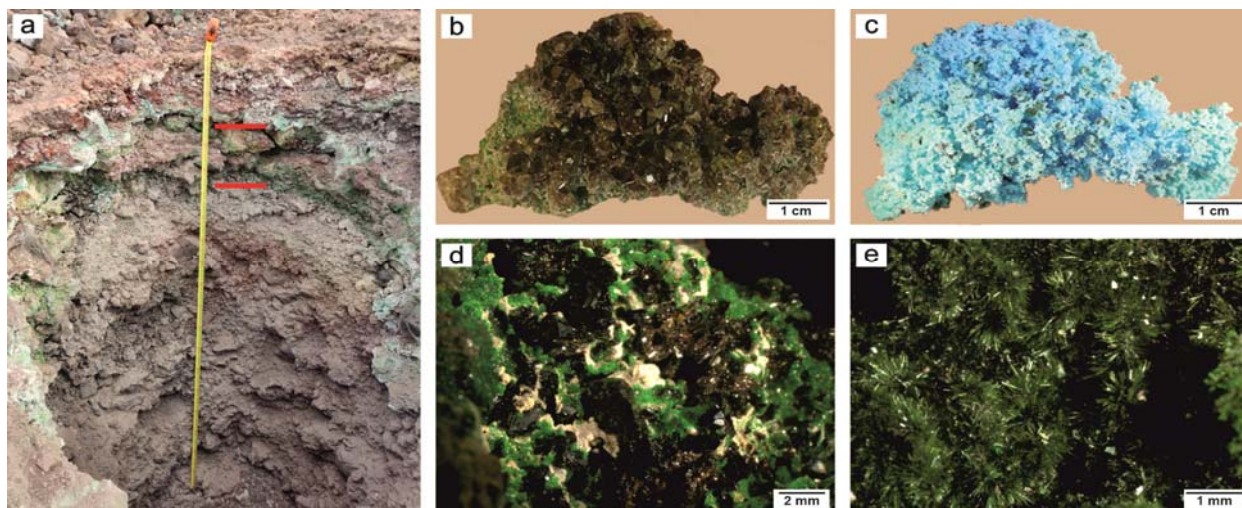


Figure 1. General view of the wall of the Yadovitaya fumarole. The Cu-SO₄ rich zone is delimited by red lines (a). The maximum thickness of the Cu-SO₄ zone is 35 cm. Well crystallized chalcocyanite sample excavated from this zone (b) and the same sample, almost completely transformed into chalcantinite, exposed to humid air for one week (c). Dark brown crystals of dolerophanite with green euchlorine (d) and clusters of needle-like crystals of alumoklyuchevskite (e) from the Cu-SO₄ zone used in this work.

Hydration experiments and high temperature powder X-ray crystallography

Experimental

Chalcocyanite, dolerophanite, alumoklyuchevskite and itelmenite are water-soluble and sensitive to air humidity. The crystals of all minerals start to alter, with initial formation of hydrated mineral films, already after one day of exposure (e.g. chalcocyanite) to open air with 81% relative humidity and 23°C. Systematic hydration experiments were carried out to monitor the occurring transformations by PXRD.

For all minerals used for further research, qualitative electron microprobe analysis (Hitachi S-3400N scanning electron microscope equipped with an Oxford Instruments X-Max 20 Energy Dispersive Spectrometer) revealed no elements other than reported in the respective publications: chalcocyanite (Siidra et al., 2018a), alumoklyuchevskite (Gorskaya et al., 1995) and itelmenite (Nazarchuk et al., 2018). There is a published semi-quantitative chemical analysis of dolerophanite

from the fumaroles of Vesuvius (Kahler, 1962). The dolerophanite sample used in this study contained 1.8 wt. % ZnO. Admixture of zinc is rather common for the copper sulfate minerals studied here. This is not surprising since the gas condensates of the GFTE were highly enriched in Zn (Menyailov et al., 1980a,b). Apart from the slight Zn for Cu substitution in dolerophanite, the ratio of the elements in the minerals agrees well with the formulas, viz. chalcocyanite $\text{Cu}(\text{SO}_4)$, dolerophanite $\text{Cu}_2\text{O}(\text{SO}_4)$, alumoklyuchevskite $\text{K}_3\text{Cu}_3\text{AlO}_2(\text{SO}_4)_4$, and itelmenite $\text{Na}_2\text{CuMg}_2(\text{SO}_4)_4$.

The experiments with all four studied minerals were carried out using the same technique: 1 g of each mineral was hand-picked under an optical microscope and ground in an agate mortar. Prior to that the purity of each sample was checked via PXRD, and in the case of observed impurities a new sample was selected. The pure powdered sample was loaded on a Si plate for further X-ray measurements. In turn, the holder with the Si plate was placed inside a common desiccator (3 liter volume). 250 ml of distilled water was poured into the bottom of the desiccator. The humidity in the desiccator during the experiments was monitored by a humidity- and temperature-meter CEM DT-625. The e.s.d. for humidity values is 0.5%. Each set of the experiments was repeated twice. In total 6 subsequent stages of hydration were carried out for each mineral and the results are listed in Tables 1,3,5. The transformation of each powder sample into the respective single phase or mixture of hydrated sulfates is accompanied by color changes (Figure 2-5).

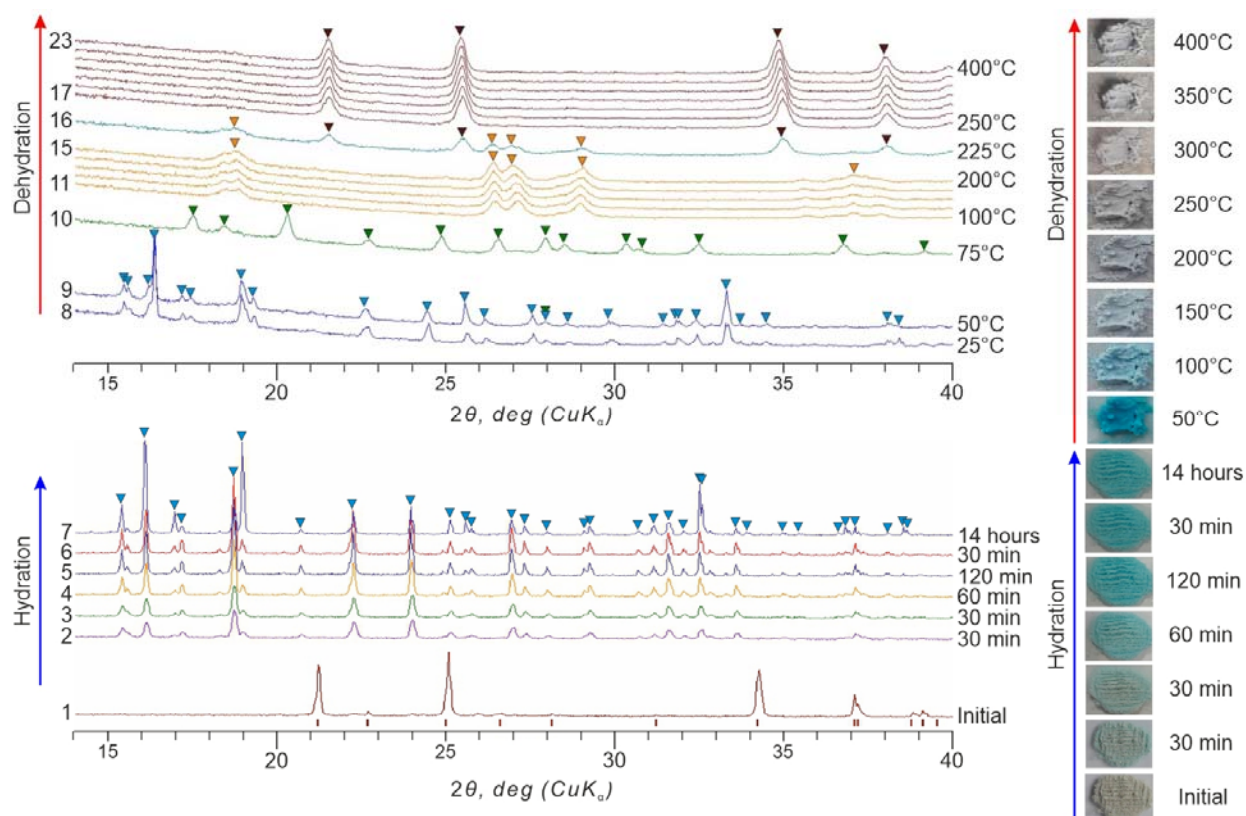


Figure 2. XRD patterns for the products of chalcocyanite hydration (left below). Different stages of hydration are numbered on the left side. Peak positions of «chalcanthite» $\text{Cu}(\text{SO}_4) \cdot 5\text{H}_2\text{O}$ are marked with ▼ triangles. XRD patterns for the products of dehydration of the mixture of hydrated sulfates initially obtained from chalcocyanite (left above). ▼ - «chalcanthite» $\text{Cu}(\text{SO}_4) \cdot 5\text{H}_2\text{O}$, ▽ - «bonattite» $\text{Cu}(\text{SO}_4) \cdot 3\text{H}_2\text{O}$, ▽ - «poitevinite» $\text{Cu}(\text{SO}_4) \cdot \text{H}_2\text{O}$, ▼ - «chalcocyanite» $\text{Cu}(\text{SO}_4)$. Hydration of chalcocyanite single-phase powder and formation of various hydrated copper sulfates is accompanied by color changes (right). During the heating of the hydrated products the color reverses back completely in agreement with the reversible hydration/dehydration of chalcocyanite. The relative humidity for each hydration stage is given in Table 1.

PXRD data in air after each stage were taken by means of a Rigaku Ultima X-ray diffractometer ($\text{CuK}\alpha$ radiation). The duration of each X-ray measurement was about 15 minutes. The evolution of the powder diffraction patterns in moist environments is shown in [Figures 2-5](#). Full powder diffraction patterns were collected at different intervals and analyzed via Rietveld refinement using the TOPAS program ([Bruker, 2014](#)). Using the known structural data for each of the intermediate phases (minerals) listed in [Tables 1-6](#) it was possible to refine the phase fraction of each of the intermediate phases and thus to determine the composition of the mixtures. Note, we put in quotes all mineral-like phases appearing during hydration/dehydration.

The thermal behavior of the mixtures of the different hydrated sulfates subsequently was studied in air by means of a Rigaku Ultima X-ray diffractometer ($\text{CoK}\alpha$ radiation (dolerophanite, alyumoklyuchevskite and itelmenite experiments) or $\text{CuK}\alpha$ radiation (chalcocyanite experiment only) and a high-temperature camera Rigaku HTA 1600. The sample was loaded on a Pt-Rh plate. Temperature steps were 25°C in the range $25\text{-}400^\circ\text{C}$. The evolution of the PXRD patterns during heating is shown in [Figures 2-5](#). The phases identified at different steps are listed in [Tables 2,4,6](#).

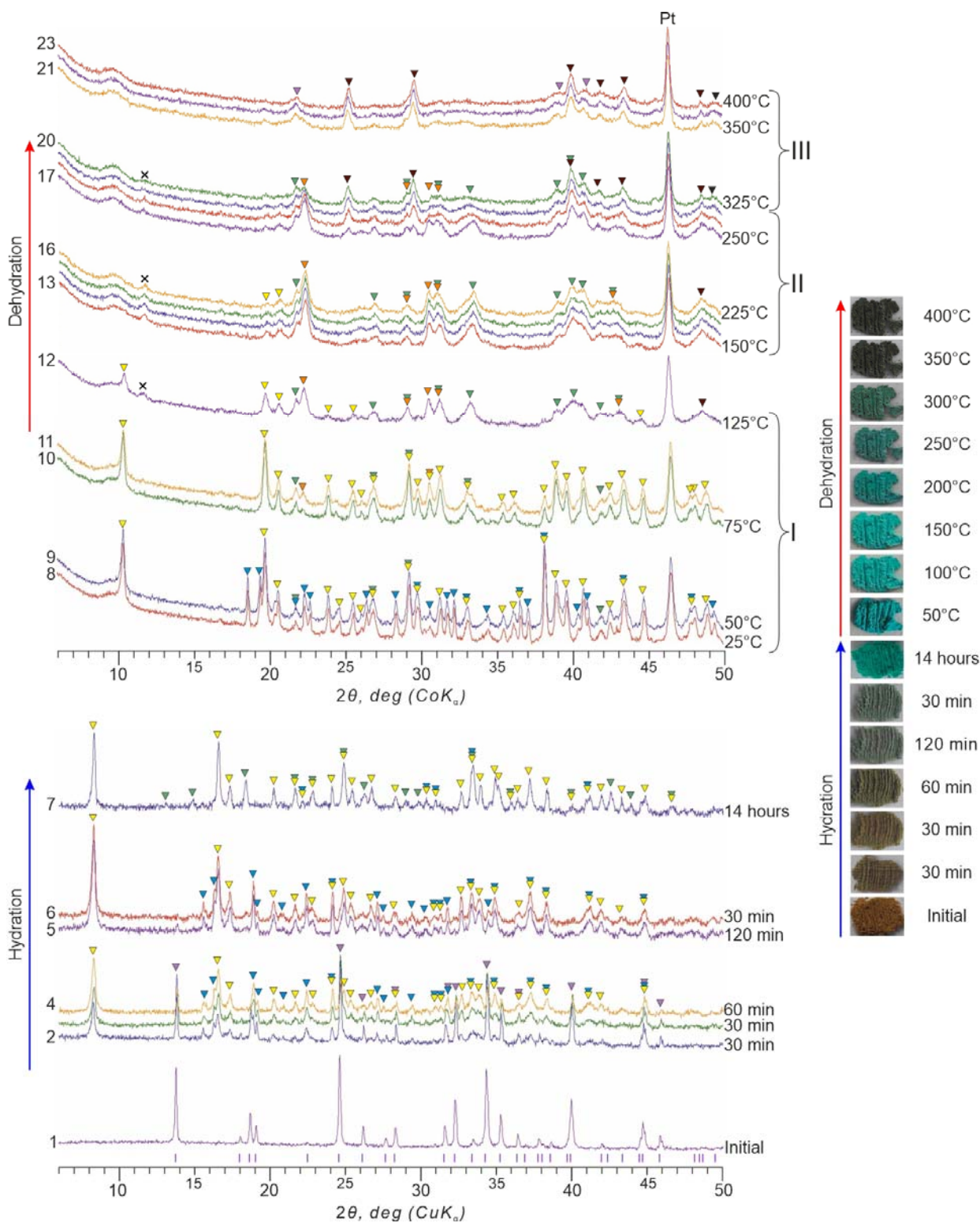


Figure 3. XRD patterns for the products of dolerophanite hydration (left below). \blacktriangledown - «dolerophanite» $\text{Cu}_2\text{O}(\text{SO}_4)$, \blacktriangledown - «chalcocyanite» $\text{Cu}(\text{SO}_4) \cdot 5\text{H}_2\text{O}$, \blacktriangledown - «kobyashevite» $\text{Cu}_5(\text{SO}_4)_2(\text{OH})_6 \cdot 4\text{H}_2\text{O}$, \blacktriangledown - «antlerite» $\text{Cu}_3(\text{SO}_4)(\text{OH})_4$. Different stages of hydration are numbered on the left side. XRD patterns for the products of dehydration of the mixture of hydrated sulfates initially obtained from dolerophanite (left above). \blacktriangledown - «dolerophanite» $\text{Cu}_2\text{O}(\text{SO}_4)$, \blacktriangledown - «chalcocyanite» $\text{Cu}(\text{SO}_4) \cdot 5\text{H}_2\text{O}$, \blacktriangledown - «kobyashevite» $\text{Cu}_5(\text{SO}_4)_2(\text{OH})_6 \cdot 4\text{H}_2\text{O}$, \blacktriangledown - «antlerite» $\text{Cu}_3(\text{SO}_4)(\text{OH})_4$, \blacktriangledown - «poitevinite» $\text{Cu}(\text{SO}_4) \cdot \text{H}_2\text{O}$, \blacktriangledown - «chalcocyanite» $\text{Cu}(\text{SO}_4)$, \blacktriangledown - CuO . Different stages of dehydration are numbered on the left side. Hydration of dolerophanite single-phase powder and formation of various hydrated copper sulfates is accompanied by color changes (right). During the heating of the hydrated products the color reverses back in agreement

with the formation of a mixture of anhydrous sulfates. The relative humidity for each hydration stage is given in Table 1.

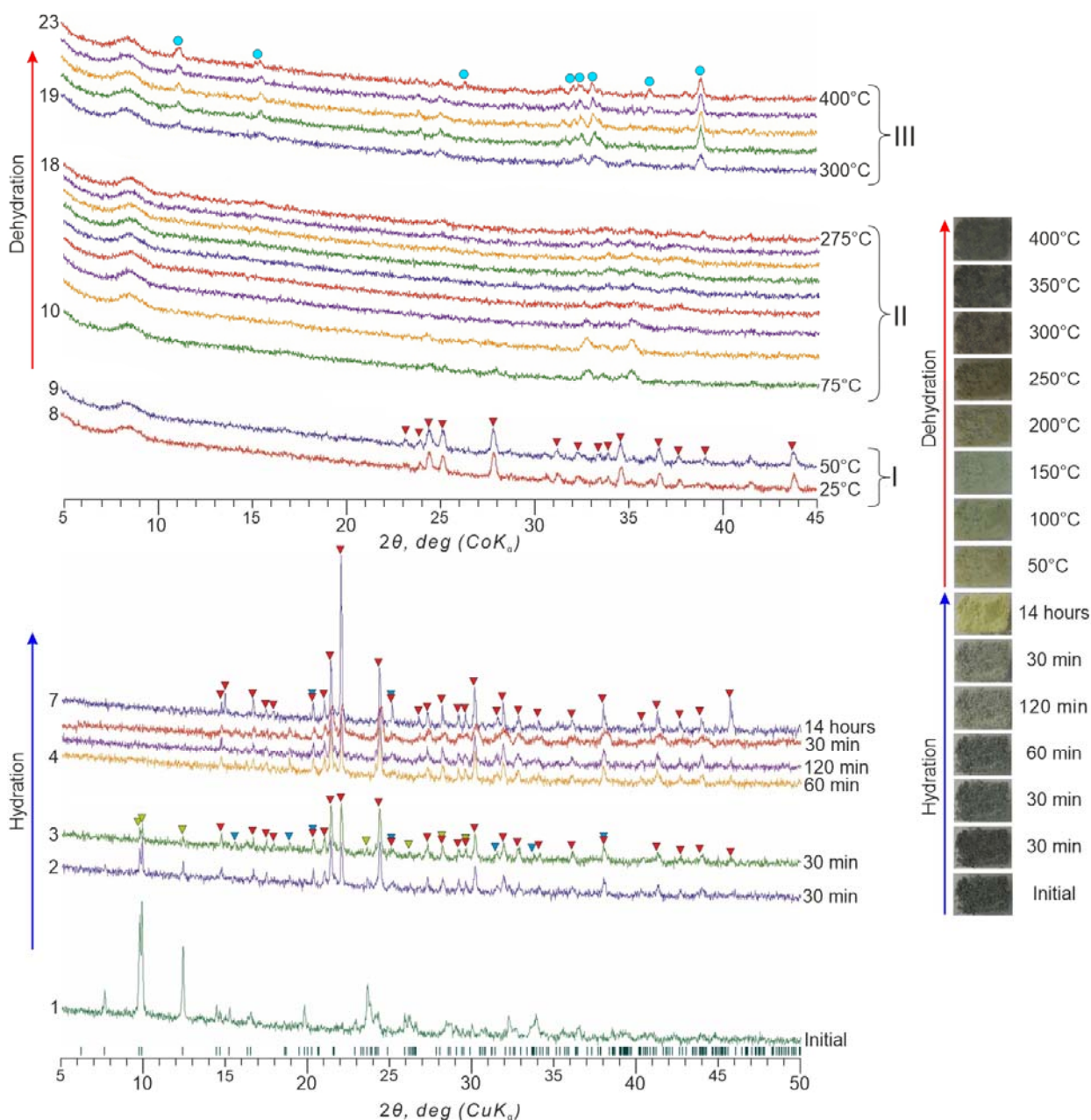


Figure 4. XRD patterns for the products of alumoklyuchevskite hydration (left below). \blacktriangledown - «alumoklyuchevskite» $\text{K}_3\text{Cu}_3(\text{Al,Fe}^{3+})(\text{SO}_4)_4\text{O}_2$, \blacktriangledown - «chalcantite» $\text{Cu(SO}_4\text{)}\cdot 5\text{H}_2\text{O}$, \blacktriangledown - «cyanochroite» $\text{K}_2\text{Cu(SO}_4\text{)}_2\cdot 6\text{H}_2\text{O}$. Different stages of hydration are numbered on the left side. XRD patterns for the products of dehydration of the mixture of hydrated sulfates initially obtained from alumoklyuchevskite (left above). \blacktriangledown - «cyanochroite» $\text{K}_2\text{Cu(SO}_4\text{)}_2\cdot 6\text{H}_2\text{O}$, \bullet - $\text{K}_2\text{Cu(SO}_4\text{)}_2$. Different stages of dehydration are numbered on the left side. Hydration of alumoklyuchevskite single-phase powder and formation of various hydrated copper sulfates is accompanied by the color changes (right). During the heating of the mixture the color partially reverses back. The relative humidity for each hydration stage is given in Table 3.

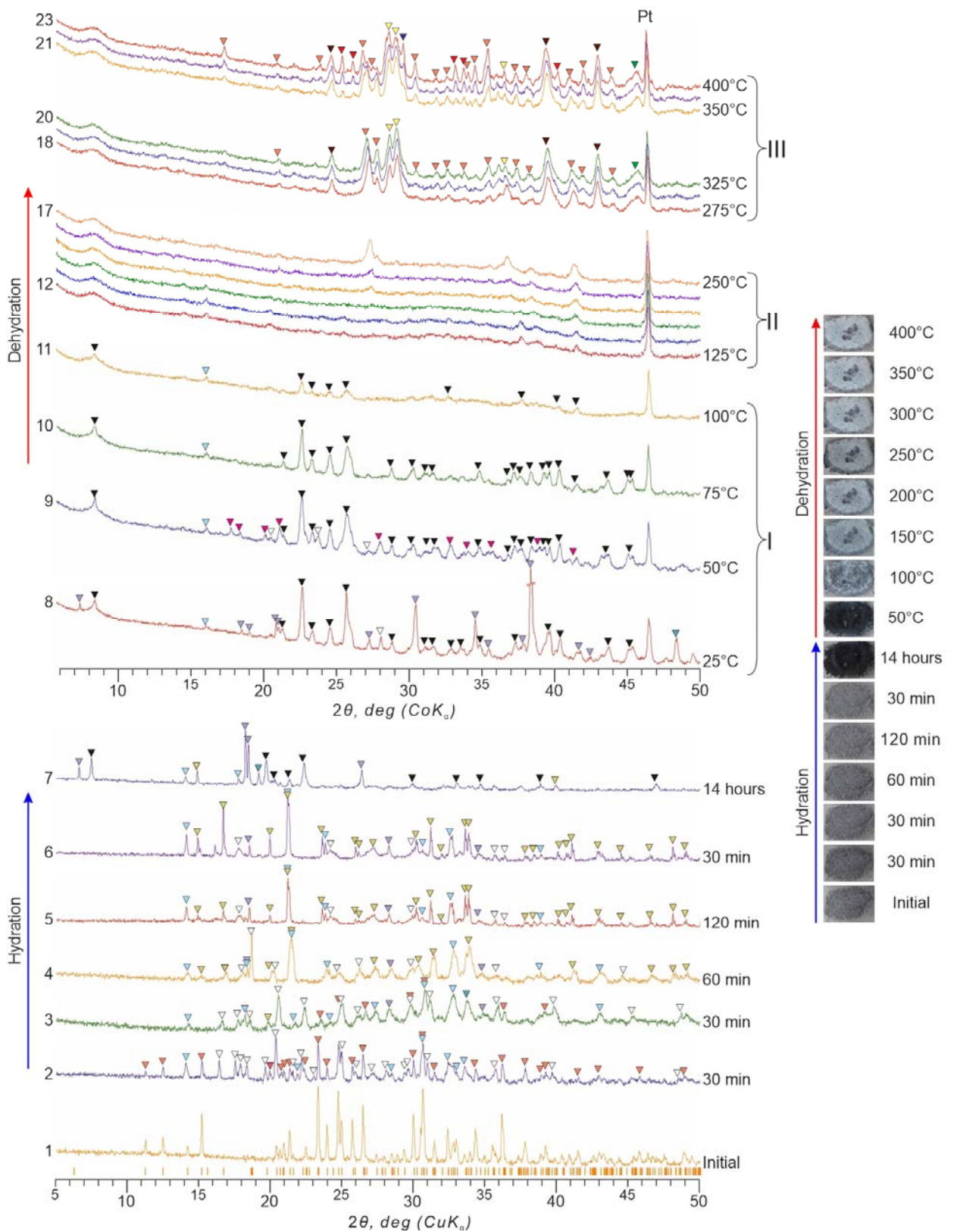


Figure 5. XRD patterns for the products of itelmenite hydration (left below). ∇ - «itelmenite» $\text{Na}_2\text{CuMg}_2(\text{SO}_4)_4$, ∇ - «hexahydrate» $\text{Mg}(\text{SO}_4) \cdot 6\text{H}_2\text{O}$, ∇ - «kröhnkite» $\text{Na}_2\text{Cu}(\text{SO}_4)_2 \cdot 2\text{H}_2\text{O}$, ∇ - «pentahydrate» $\text{Mg}(\text{SO}_4) \cdot 5\text{H}_2\text{O}$, ∇ - «brucite» $\text{Mg}(\text{OH})_2$, ∇ - «epsomite» $\text{Mg}(\text{SO}_4) \cdot 7\text{H}_2\text{O}$, ∇ - «konyaite» $\text{Na}_2\text{Mg}(\text{SO}_4)_2 \cdot 5\text{H}_2\text{O}$, ∇ - «alpersite» $(\text{Mg,Cu})(\text{SO}_4) \cdot 7\text{H}_2\text{O}$. Different stages of hydration are numbered on the left side. XRD patterns for the products of dehydration of the mixture of hydrated sulfates initially obtained from itelmenite (left above). ∇ - «itelmenite» $\text{Na}_2\text{CuMg}_2(\text{SO}_4)_4$, ∇ - «hexahydrate» $\text{Mg}(\text{SO}_4) \cdot 6\text{H}_2\text{O}$, ∇ - «kröhnkite» $\text{Na}_2\text{Cu}(\text{SO}_4)_2 \cdot 2\text{H}_2\text{O}$, ∇ - «brucite» $\text{Mg}(\text{OH})_2$, ∇ - «konyaite» $\text{Na}_2\text{Mg}(\text{SO}_4)_2 \cdot 5\text{H}_2\text{O}$, ∇ - «alpersite» $(\text{Mg,Cu})(\text{SO}_4) \cdot 7\text{H}_2\text{O}$.

▼ - «Cu-pentahydrate» $(\text{Mg}_{0.4}\text{Cu}_{0.6})(\text{SO}_4) \cdot 5\text{H}_2\text{O}$, ▼ - MgO, ▼ - $\text{Mg}(\text{SO}_4)$, ▼ - «chalcocyanite» $\text{Cu}(\text{SO}_4)$, ▼ - «vanthoffite» $\text{Na}_6\text{Mg}(\text{SO}_4)_4$, ▼ - «metathenardite» $\text{Na}_2(\text{SO}_4)$. Different stages of dehydration are numbered on the left side. Hydration of itelmenite single-phase powder and formation of various hydrated copper and magnesium sulfates is accompanied by the color changes (right). During the heating of the mixture the color reverses back. The relative humidity for each hydration stage is given in Table 5.

Results

I. Chalcocyanite $\text{Cu}(\text{SO}_4)$

Hydration

In moist atmosphere chalcocyanite transforms rapidly into «chalcanthite» $\text{Cu}(\text{SO}_4) \cdot 5\text{H}_2\text{O}$ (Bacon and Titterton, 1975). The single-phase composition remains intact until the last stage of the hydration (Figure 2).

Dehydration

The first stage of heating (Figure 2) at 25°C and 50°C is also characterized by the predominantly single-phase chalcanthite composition of the probe. However, we should note that first minor peaks of «bonattite» $\text{Cu}(\text{SO}_4) \cdot 3\text{H}_2\text{O}$ (Zahrobsky and Baur, 1968) start to appear at 50°C. At 75°C, the sample completely consists of «bonattite» $\text{Cu}(\text{SO}_4) \cdot 3\text{H}_2\text{O}$. The third stage covers the relatively large temperature range 100°C - 200°C and is characterized also by a single-phase corresponding to «poitevinite» $\text{Cu}(\text{SO}_4) \cdot \text{H}_2\text{O}$ (Giester et al., 1994). At 225°C a transitional stage with coexisting poitevinite and anhydrous CuSO_4 (chalcocyanite) is observed. Starting from 250°C the sample composition has reversed back to the initial chalcocyanite. The color of the powder sample is also the initial grey (Figure 2).

II. Dolerophanite $\text{Cu}_2\text{O}(\text{SO}_4)$

Hydration

The initial dolerophanite sample contained no admixtures of other phases (Figure 3) and its powder pattern corresponds to that reported for synthetic $\text{Cu}_2\text{O}(\text{SO}_4)$ (Effenberger, 1985).

After the hydration processes have started, the phase composition undergoes significant transformations (diffraction patterns 2-4 in Figure 4). «Kobayashevite» $\text{Cu}_5(\text{SO}_4)_2(\text{OH})_6 \cdot 4\text{H}_2\text{O}$ (Pekov et al., 2013) and «chalcanthite» $\text{Cu}(\text{SO}_4) \cdot 5\text{H}_2\text{O}$ (Bacon and Titterton, 1975) appear in significant amounts. The amount of dolerophanite gradually decreases, and drops down to 13 wt.% as registered in powder pattern #4.

At the next stage of hydration (diffraction patterns 5-6 in Figure 3 and Table 1) the signature of dolerophanite has almost disappeared, and its amount is refined to yield only 3 wt. %. «Kobayashevite» has become the major phase with 67 wt. % whereas the «chalcanthite» content is still important with ~30 wt. %.

The last stage of the dolerophanite hydration experiment (diffraction pattern 7 in Figure 3 and Table 1) is characterized by the almost complete disappearance of «chalcanthite» in favour of «antlerite», $\text{Cu}_3(\text{SO}_4)(\text{OH})_4$ (Hawthorne et al., 1989). The remains of «chalcanthite» amount to only ~ 6 wt. %.

Dehydration

The dolerophanite dehydration processes with increasing temperature can be classified into three main stages (Table 2). The characteristic of stage I is the dominance of «kobyashevite» although its amount gradually decreases with rising temperature. Diffraction patterns 10-12 at 75°C, 100°C and 125°C (Figure 3) demonstrate the appearance of «poitevinite» $\text{Cu}(\text{SO}_4)\cdot\text{H}_2\text{O}$ (Ting et al., 2009) at the expense of the «chalcanthite».

The dehydration stage II, starting at 150°C, is characterized by the complete disappearance of «kobyashevite», with «poitevinite» and «antlerite» becoming the dominant phases. Minor amounts of «chalcocyanite» (~3 wt. %) appear in the polyphasic mixture. The «poitevinite» amount gradually decreases with rising temperature till 300°C. The amount of «antlerite» remains nearly constant during this process, but the amount of chalcocyanite gradually increases.

The last dehydration stage III starts at 325°C and is accomplished at 350°C. «Chalcocyanite» is the dominant phase throughout this stage with about 70%. Re-appearance of «dolerophanite» is observed at this temperature, but its amount does not exceed 20%. «Tenorite» CuO (Brese et al., 1990) is present with about 12% as an obvious product of decomposition of «chalcocyanite» and/or «dolerophanite». The color of the sample becomes brownish at the end (Figure 3).

Table 1. Evolution of primary dolerophanite into mixtures of hydrated sulfates during the hydration experiments at 23°C, different duration and different relative humidity. The amount of each phase is given in wt. %. E.s.d is ~3%.

Initial sample Stage 1	Stage 2 30 minutes, humidity 85%	Stage 3 30 minutes, humidity 86%	Stage 4 60 minutes, humidity 88%	Stage 5 120 minutes, humidity 90%	Stage 6 30 minutes, humidity 91%	Stage 7 14 hours, humidity 94%
dolerophanite 100	«dolerophanite» 47 «kobyashevite» 28 «chalcanthite» 25	«kobyashevite» 41 «dolerophanite» 31 «chalcanthite» 28	«kobyashevite» 58 «chalcanthite» 29 «dolerophanite» 13	«kobyashevite» 67 «chalcanthite» 30 «dolerophanite» 3	«kobyashevite» 67 «chalcanthite» 30 «dolerophanite» 3	«kobyashevite» 67 «antlerite» 27 «chalcanthite» 6

Table 2. Evolution of the mixture of hydrated sulfate phases, formed as a result of dolerophanite hydration, upon heating. Dominating phases ($\geq 20\%$) are marked in bold. Amount of each phase is given in wt. %. E.s.d is ~3%.

I				II			
+25	+50	+75	+100	+125	+150	+175	+200
«kobyashevite» 63 «chalcanthite» 29 «antlerite» 8	«kobyashevite» » 62 «chalcanthite» 29 «antlerite» 9	«kobyashevite» 73 «poitevinite» 17 «antlerite» 10	«kobyashevite» 68 «poitevinite» 22 «antlerite» 10	«kobyashevite» 49 «poitevinite» 39 «antlerite» 10 «chalcocyanite» 2	«poitevinite» 67 «antlerite» 27 «chalcocyanite» 3 «kobyashevite» 3	«poitevinite» 69 «antlerite» 27 «chalcocyanite» 2 «kobyashevite» 2	«poitevinite» 67 «antlerite» 28 «chalcocyanite» 3 «kobyashevite» 2
II				III			
+225	+250	+275	+300	+325	+350	+375	+400
«poitevinite» 63 «antlerite» 31	«poitevinite» 49 «antlerite» 33	«poitevinite» 39 «antlerite» 32 «chalcocyanite» » 29	«poitevinite» 38 «antlerite» 33 «chalcocyanite» » 29	«chalcocyanite» » 40 «antlerite» 29 «poitevinite» 29	«chalcocyanite» 68 «dolerophanite» » 20	«chalcocyanite» » 69 «dolerophanite» 19	«chalcocyanite» » 69 «dolerophanite» 18

«chalcocyanite» 5 «kobyashevite» 1	«chalcocyanite» 18			«tenorite» 2	«tenorite» 12	«tenorite» 12	«tenorite» 13
---------------------------------------	--------------------	--	--	--------------	---------------	---------------	---------------

III. Alumoklyuchevskite $K_3Cu_3AlO_2(SO_4)_4$

Hydration

The initial alumoklyuchevskite sample contained no detected admixtures of other phases (Figure 4) and its powder pattern is in a good agreement with that calculated for its recently refined crystal structure (Siidra et al. 2017).

Immediately after the start of hydration, the alumoklyuchevskite sample starts to decompose and shows the diffraction pattern of two hydrated phases (diffraction patterns 2 and 3 in Figure 4): «cyanochroite» $K_2Cu(SO_4)_2 \cdot 6H_2O$ (Bosi et al., 2009) and subordinate «chalcantite» $Cu(SO_4) \cdot 5H_2O$ (Bacon and Titterton, 1975). After 60 minutes of hydration, the reflections of alumoklyuchevskite have completely disappeared. The amount of «cyanochroite» gradually increases, and at the end of hydration, the sample is almost completely represented by this phase (diffraction pattern 7 in Figure 4; Table 3).

Dehydration

The dehydration behavior of the product of the alumoklyuchevskite hydration registered by PXRD appears relatively simple. It is characterized by three main stages (Table 4). At the beginning of experiment, when the temperature reached 25°C, the remains of «chalcantite» have completely disappeared and only diffraction peaks of «cyanochroite» are present. According to the diffraction patterns 10-18 in Figure 4, the sample undergoes gradual amorphization.

A recrystallization of the sample is observed in the range 300-400°C. All the observed peaks correspond to $K_2Cu(SO_4)_2$ (PDF card No. 00-017-0485). The crystal structure of this phase is unknown. $K_2Cu(SO_4)_2$, reported recently by Zhou et al. (2020), has unrelated PXRD pattern.

Note that despite the likely formation of a considerable amount of crystalline «cyanochroite» during hydration, the color of the resulting sample does not show the typical bluish tints typical for the mineral cyanochroite, but the color appears yellow with greenish tints instead. This might be an indication of the amorphous Al_2O_3 or its hydrated forms as decomposition products which envelop the finely dispersed crystallites of «cyanochroite».

Table 3. Evolution of primary alumoklyuchevskite into mixtures of hydrated sulfates during the hydration experiments at 23°C, different duration and different relative humidity. The amount of each phase is given in wt. %. E.s.d is ~3%.

Initial sample Stage 1	Stage 2 30 minutes, humidity 85%	Stage 3 30 minutes, humidity 86%	Stage 4 60 minutes, humidity 88%	Stage 5 120 minutes, humidity 90%	Stage 6 30 minutes, humidity 91%	Stage 7 14 hours, humidity 94%
alumoklyuchevskite 100	«cyanochroite» 82 «alumoklyuchevskite» 13	«cyanochroite» 86 «chalcantite» 9	«cyanochroite» 89	«cyanochroite» 90	«cyanochroite» 81	«cyanochroite» 98 «chalcantite» 2

	«chalcanthite» 5	«alumoklyuchevskite» 5	«chalcanthite» 11	«chalcanthite» 10	«chalcanthite» 19	
--	------------------	------------------------	-------------------	-------------------	-------------------	--

Table 4. Evolution of the mixture of hydrated sulfate phases, formed as a result of alumoklyuchevskite hydration, upon heating. Dominating phases ($\geq 20\%$) are marked in bold. The transformation can be subdivided into three main stages (I - III) in accordance with the dominance of different phases (marked in bold). Amount of each phase is given in wt. %. E.s.d is $\sim 3\%$.

I		II								III					
+25	+50	+75	+100	+125	+150	+175	+200	+225	+250	+275	+300	+325	+350	+375	+400
«cyanochroite» 100	«cyanochroite» 100	Amorphization stage								«K₂Cu(SO₄)» 100					

IV. Itelmenite $\text{Na}_2\text{CuMg}_2(\text{SO}_4)_4$

Hydration

The initial itelmenite sample contained no admixtures of other phases (Figure 5) and its powder pattern is in a good agreement with the pattern calculated for the crystal structure of itelmenite (Nazarchuk et al., 2018).

Itelmenite demonstrates remarkably complex and multiple transformations even after the first 30 minutes of hydration. About half of the polyphase mixture is still represented by itelmenite. The second most significant phase is «hexahydrate» $\text{Mg}(\text{SO}_4) \cdot 6\text{H}_2\text{O}$ (Zalkin et al., 1964). The other hydrates of magnesium sulfates are represented by «pentahydrate» $\text{MgSO}_4 \cdot 5\text{H}_2\text{O}$ (Baur and Rolin, 1972), «starkeyite» $\text{Mg}(\text{SO}_4) \cdot 4\text{H}_2\text{O}$ (Baur, 1962) and «sanderite» $\text{Mg}(\text{SO}_4) \cdot 2\text{H}_2\text{O}$ (Ma et al., 2009). «Kröhnkite» $\text{Na}_2\text{Cu}(\text{SO}_4)_2 \cdot 2\text{H}_2\text{O}$ (Hawthorne and Ferguson, 1975) and «brucite» $\text{Mg}(\text{OH})_2$ (Mitev et al., 2009) are also present in minor amounts (Table 5).

After another 30 minutes of hydration the amount of itelmenite is reduced. «Kröhnkite» becomes dominant and the amount of «hexahydrate» is reduced. New phases «epsomite» $\text{Mg}(\text{SO}_4) \cdot 7\text{H}_2\text{O}$ (Calleri et al., 1984) and «alpersite» $(\text{Mg,Cu})(\text{SO}_4) \cdot 7\text{H}_2\text{O}$ (Mills et al., 2010) appear in minor amounts.

The third stage of hydration (diffraction patterns 4-6 in Figure 5) is characterized by almost constant phase composition, with only slight variations in the amounts of these phases. Primary itelmenite no longer exists in the mixture, and only «kröhnkite», «epsomite», «hexahydrate» and «alpersite» are registered.

The last stage of hydration is characterized by the strong shift of the dominant phases and appearance of «konyaite» $\text{Na}_2\text{Mg}(\text{SO}_4)_2 \cdot 5\text{H}_2\text{O}$ (Mills et al., 2010) in the amount of 62 wt.%.

Dehydration

At 25°C and 50°C the composition of the polyphase sample, with «konyaite» as the dominant phase, is similar to the final stage of hydration. At 75°C the sample completely transforms into a two-phase mixture highlighting the end of the dehydration stage I.

The dehydration stage **II** indicates almost complete amorphization of the sample (diffraction patterns 12-17 in Figure 5). Some relics of crystalline matter are present, but an interpretation of the diffraction pattern is uncertain.

The dehydration stage **III** is characterized by the presence of anhydrous crystalline phases only. Simple $Mg(SO_4)$ (Rentzeperis and Soldatos, 1958) is the dominant phase in the range from 275°C to 375°C. Its amount gradually reduces with the rise of the temperature in favour of the amount of «chalcocyanite» $Cu(SO_4)$. Already at 275°C itelmenite reappears in minor amounts and becomes the dominant phase at 400°C. «Vanthoffite» $Na_6Mg(SO_4)_4$ (Fischer and Hellner, 1964), «metathénardite» $Na_2(SO_4)$ (Rasmussen et al., 1996) and MgO (Fan et al., 2008) are minority phases.

In the photographs (Figure 5), it is clearly seen that the initial gray color of the itelmenite powder sample fades away towards the end of the experiment and its color becomes light-gray.

Table 5. Evolution of primary itelmenite into mixtures of hydrated sulfates during the hydration experiments at 23°C, different duration and different relative humidity. The amount of each phase is given in wt. %. E.s.d is ~3%.

Initial sample Stage 1	Stage 2 30 minutes, humidity 85%	Stage 3 30 minutes, humidity 86%	Stage 4 60 minutes, humidity 88%	Stage 5 120 minutes, humidity 90%	Stage 6 30 minutes, humidity 91%	Stage 7 14 hours, humidity 94%
itelmenite 100	«itelmenite» 48 «hexahydrate» 35 «kröhnkite» 8 «pentahydrate» 3 «sanderite» 3 «starkeyite» 2 «brucite» 1	«kröhnkite» 34 «itelmenite» 31 «hexahydrate» 24 «alpersite» 6 «brucite» 3 «epsomite» 2	«epsomite» 66 «kröhnkite» 24 «hexahydrate» 7 «alpersite» 3	«kröhnkite» 46 «epsomite» 42 «hexahydrate» 9 «alpersite» 3	«epsomite» 52 «kröhnkite» 44 «hexahydrate» 2 «alpersite» 2	«konyaite» 62 «alpersite» 31 «kröhnkite» 3 «epsomite» 3 «brucite» 1

Table 6. Evolution of the mixture of hydrated sulfate phases, formed as a result of itelmenite hydration, upon heating. Dominating phases ($\geq 20\%$) are marked in bold. The evolution can be subdivided into three main stages (I - III) in accordance with the dominance of different phases (marked in bold). Amount of each phase is given in wt. %. E.s.d is ~3%.

I				II					
+25	+50	+75	+100	+125	+150	+175	+200	+225	+250
«konyaite» 68 «alpersite» 29 «brucite» 2 «epsomite» 1	«konyaite» 68 «Cu-pentahydrate» 19 «hexahydrate» 8 «kröhnkite» 5	«kröhnkite» 90 «konyaite» 10	«kröhnkite» 75 «konyaite» 25	Amorphization					
III									
+275	+300	+325	+350	+375	+400				
$MgSO_4$ 70 «chalcocyanite» 23 «itelmenite» 6 MgO 1	$MgSO_4$ 69 «chalcocyanite» 23 «itelmenite» 7 MgO 1	$MgSO_4$ 50 «chalcocyanite» 29 «itelmenite» 16 MgO 2 «vanthoffite» 2 «metathénardite» 1	$MgSO_4$ 45 «itelmenite» 29 «chalcocyanite» 21 MgO 2 «vanthoffite» 2 «metathénardite» 1	$MgSO_4$ 39 «itelmenite» 35 «chalcocyanite» 16 «vanthoffite» 7 MgO 2 «metathénardite» 1	«itelmenite» 38 $MgSO_4$ 37 «chalcocyanite» 13 «vanthoffite» 10 MgO 1 «metathénardite» 1				

Discussion

Chalcocyanite. The reversible hydration of this mineral has been studied previously using synchrotron radiation (Ting et al., 2009). The good agreement of our results with those reported by (Ting et al., 2009) makes us confident that our experimental setup reproduces the hydration process of this mineral sufficiently well. Thus, chalcocyanite can be relied on as a reference system for the other minerals studied in this work. Under high RH (relative humidity) at ambient conditions, hydration proceeds in one step yielding the thermodynamically stable product, *i.e.* chalcantite. The small amount of chalcocyanite remaining even after several hours of hydration can be probably explained by formation of chalcantite “shells” around the initial chalcocyanite particles which block or strongly retard the hydration process. On heating, formation of the less water-rich forms proceeds in the temperature intervals which agree well with the data of (Cheng et al. 2019). Note the relatively low crystallinity of the monohydrate.

Dolerophanite. Hydration. This case is more complex than the previous one as the hydration involves formation of basic copper sulfates whose interconversion depends on a variety of external conditions including temperature, presence of liquid phase and its acidity as well as copper concentration (Yoder et al. 2007; Stanimirova and Ivanova, 2019). The first step of hydration can be described tentatively by an equation $3\text{Cu}_2\text{O}(\text{SO}_4) + 14\text{H}_2\text{O} = \text{Cu}_5(\text{SO}_4)_2(\text{OH})_6 \cdot 4\text{H}_2\text{O} + \text{Cu}(\text{SO}_4) \cdot 5\text{H}_2\text{O}$, or expressed in shorthand by the Cu:SO₄ ratio, 3(2:1) = (1:1) + (5:2). The (5:2) compound is known to be easily formed either by reaction of CuO with an aqueous solution of CuSO₄ (Stanimirova and Ivanova, 2019) or gently increasing the pH of a CuSO₄ solution by adding small amounts of alkalis (Yoder et al. 2007), probably due to kinetic reasons. It was found to be stable in contact with aqueous solutions of cupric sulfate (1M or slightly below), while in pure water it readily converts into brochantite (4:1) or its hydrates (posnyakovite and langite). In addition, Yoder et al. (2007) note that in their experiments, antlerite (3:1) could only be obtained at 80°C or above. Yet, in our case the kobyashevite as the major hydration product of dolerophanite was in steady contact with a slurry containing solid chalcantite, *i.e.* copper sulfate pentahydrate, during the hydration process. Note that Yoder et al. (2007) studied the stability of kobyashevite only against 1M Cu(SO₄) and pure water; other concentrations of cupric sulfate solution may well lead to formation of antlerite already at room temperature. Further investigations of basic copper sulfate interconversions in copper sulfate solutions of varied concentrations, including the presence of solid Cu(SO₄)·5H₂O, are obviously necessary to provide better understanding of these processes.

Formation of synthetic kobyashevite was also detected upon hydration of a more complex copper oxysulfate mineral, euchlorine KNaCu₃O(SO₄)₂ (Siidra et al. 2019a), but formation of antlerite was not observed. Possibly, the concentration of copper sulfate in the slurries formed was

not high enough because of the relatively low solubility of krönkite-type double copper – alkali sulfate products.

Dehydration. Evaporation of water from the initial slurry results in the initial crystallization of dissolved chalcantite. In agreement with Yoder et al. (2007), the antlerite content increases as the temperature rises and water-rich kobyashevite dehydrates. This step can be described by a tentative equation $2\text{Cu}_5(\text{SO}_4)_2(\text{OH})_6 \cdot 4\text{H}_2\text{O} = 3\text{Cu}_3(\text{SO}_4)(\text{OH})_4 + \text{Cu}(\text{SO}_4) \cdot \text{H}_2\text{O} + 7\text{H}_2\text{O}$, or in shorthand, $2(5:2) = 3(3:1) + (1:1)$. Poitevnite is also formed by dehydration of chalcantite. At the final steps, copper hydroxyl sulfates decompose with loss of water and formation of cyanochroite and tenorite. We note that, while our study was restricted to 450°C, the suggested deposition temperature on the wall of the fumarole, only a small part of the initial dolerophanite was recovered. In the thermoanalytical studies dedicated to dehydration of basic copper sulfates (Ramamurthy and Secco, 1970; Uzunov et al. 1985; Tanaka and Koga 1988), thermal effects attributed to the formation of synthetic dolerophanite (in a CuO-rich mixture) are reported to occur at somewhat higher temperatures (around 500°C). In one of our test experiments in a sealed silica tube no reaction was observed between CuO and Cu(SO₄) up to 550°C. In contrast, formation of basic copper *alkali* sulfates proceeds easily below 450°C both upon dehydration (Siidra et al. 2019a) and *in silico*.

Alumoklyuchevskite. The chemical identity of at least some of the hydration products remains obscure due to their amorphous nature. Based on the crystalline products formed at the first stage, we may suggest the following equation: $2\text{K}_3\text{Cu}_3\text{AlO}_2(\text{SO}_4)_4 + (26+x)\text{H}_2\text{O} = 3\text{K}_2\text{Cu}(\text{SO}_4)_2 \cdot 6\text{H}_2\text{O} + \text{Cu}(\text{SO}_4) \cdot 5\text{H}_2\text{O} + [\text{Al}_2(\text{SO}_4)(\text{OH})_4 \cdot x\text{H}_2\text{O}]$, the amorphous part (with a tentative composition) shown in brackets. The low temperature of the hydration process probably favors formation of amorphous basic aluminum salts which crystallize with difficulty, as noted particularly for sulfates (Nordstrom, 1982). It is possible that the progressive disappearance of chalcantite is caused by its slow dissolution in the slurry (it is more water soluble compared to cyanochroite) and sorption by the aluminum-based amorphous phase. Further reactions involving formation of amorphous double copper-aluminum hydroxysulfates are also possible.

Upon heating, given the overall cation ratio, one could expect formation of sulfates with K:Cu ratio of 1:1, i.e. $\text{K}_2\text{Cu}_2(\text{SO}_4)_3$ (Lander et al. 2017), or a mixture of $\text{K}_2\text{Cu}(\text{SO}_4)_2$ and $\text{Cu}(\text{SO}_4)$. Instead, the only process detectable by PXRD study is dehydration of cyanochroite, also via an amorphous precursor. TG-DTA studies of synthetic cyanochroite (Nagase et al. 1978) revealed a two-step loss of water (which is complete below 150°C) followed by two endothermal effects at 370 and 520°C, the latter being attributed to melting. The yet not interpreted data provided in the PDF card No. 00-017-0485 refer to the compound prepared by dehydration of cyanochroite, most likely to the high-temperature form of $\text{K}_2\text{Cu}(\text{SO}_4)_2$ while the structure reported by Zhou et al.

(2020) refers to its low-temperature form, according to the way of preparation. In our experiment, crystallization of the high-temperature form starts from $\sim 275^\circ\text{C}$ which might be enhanced by the amorphous nature of the precursor or by the presence of aluminum. Detailed temperature-dependent studies of $\text{K}_2\text{Cu}(\text{SO}_4)_2 \cdot 6\text{H}_2\text{O}$ and its anhydrous form, particularly DTA/PXRD, are evidently necessary to confirm the nature of compound noted in the PDF card No. 00-017-0485.

Itelmenite. Due to the absence of additional oxygen atoms, the formation of any basic salts upon hydration is not expected. Only a few selected and partial studies have been performed within the relatively complex $\text{Na}_2(\text{SO}_4) - \text{Cu}(\text{SO}_4) - \text{Mg}(\text{SO}_4) - \text{H}_2\text{O}$ system (e.g. Steiger et al., 2011; Lindström et al., 2016). In addition, rapid hydration is most likely driven by kinetic factors, *i.e.* compounds more easily formed are observed first. Hence, the initial hydration stage can be described by the following tentative equation: $\text{Na}_2\text{CuMg}_2(\text{SO}_4)_4 + (2+2x)\text{H}_2\text{O} = \text{Na}_2\text{Cu}(\text{SO}_4)_2 \cdot 2\text{H}_2\text{O} + 2(\text{Mg,Cu})(\text{SO}_4) \cdot x\text{H}_2\text{O}$. The latter formula designates the successively formed magnesium sulfates which may also accommodate the remaining copper sulfate as the latter's hydrates are not observed. The following steps correspond mostly to progressive hydration of Mg/Cu sulfates until the point where the largest hydration point is observed (epsomite and alpersite). Further reactions are likely to proceed in partially deliquesced samples: dissolution of kröhnkite and epsomite leads to formation of konyaite; the released cupric sulfate contributes to alpersite which forms also at the expense of epsomite: $\text{Na}_2\text{Cu}(\text{SO}_4)_2 \cdot 2\text{H}_2\text{O} + 3\text{Mg}(\text{SO}_4) \cdot 7\text{H}_2\text{O} + 3\text{H}_2\text{O} = \text{Na}_2\text{Mg}(\text{SO}_4)_2 \cdot 5\text{H}_2\text{O} + 3\text{Mg}_{0.67}\text{Cu}_{0.33}(\text{SO}_4) \cdot 7\text{H}_2\text{O}$. This reaction is partially reversed on heating when water starts to evaporate. Partial dehydration of alpersite also contributes to the transient cuprian pentahydrate. As in the previous case, decomposition of complex mixture of hydrates results in amorphization (partial dissolution?). It is therefore not possible to trace the origin of crystalline phases arising at $\sim 275^\circ\text{C}$. The last step is characterized by a slow reaction of anhydrous sulfates with formation of the initial itelmenite, probably enhanced by the seed crystals formed from the amorphous precursor. The small amount of $\text{Mg}(\text{OH})_2$ formed due to partial hydrolysis converts independently into MgO.

Structural evolution

The analysis of the sequential phase formation shows that the behavior of the studied minerals differs significantly (Figures 6, 7). The formulas and structures of hydrates, formed as a result of chalcocyanite transformations during hydration and subsequent heating, are more complex than the initial simple copper sulfate CuSO_4 . The opposite behavior, namely the formation of simpler phases during hydration, was recently described in our study of euchlorine (Siidra et al., 2019a). To analyze quantitatively the sequence of transformations of mineral phases, we performed an analysis of their structural complexity, I_G in bits/atom, using the approach

proposed in Krivovichev (2013). Additionally, for each of the minerals, weighted average values of I_G bits/atom at each stage of the experiment were calculated (Figure 6), using molar fraction of each mineral phase (where x_i – molar fraction, w_i – weight %, M_i – molar mass, of i phase, respectively).

In the case of chalcocyanite (2.252 bits/atom) (Figure 6a) and dolerophanite (2.750 bits/atom) (Figure 6b), the complexity increases due to the fact that even simple copper sulfate hydrated offsprings have a higher structural complexity than their anhydrous analogues. This is in agreement with a common structural trend (Krivovichev, 2014). Illustrative examples are anhydrite $\text{Ca}(\text{SO}_4)$ (1.918 bits/atom) and gypsum $\text{Ca}(\text{SO}_4) \cdot 2\text{H}_2\text{O}$ (2.752 bits/atom).

The structural complexity of the phases (cyanochroite and chalcantite) formed during hydration of the alumoklyuchevskite (Figure 6c) is lower than that of the initial mineral. As noted above, there are currently no structural data on the « $\text{K}_2\text{Cu}(\text{SO}_4)_2$ » phase (PDF card No. 00-017-0485) available, thus the structural complexity could not be estimated for the final stage.

In an experiment with itelmenite, the weighted average structural complexity of the phases formed also decreases, however, by the end of dehydration, having passed through the amorphous state stage, when anhydrous sulfates are formed at high temperatures, its value increases again (Figure 7a).

The phases resulting from hydration and subsequent dehydration of euchlorine (Figure 7b) demonstrate a significant reduction in structural complexity with respect to the initial phase. However, by the end of the experiment, as the phase composition of the sample returns to the initial, almost single-phase euchlorine composition, the weighted average structural complexity becomes close to the initial value.

Thus, the performed analysis shows that many of the primary exhalative Cu^{2+} -containing sulfates are structurally intermediate complex (Krivovichev, 2013). Alumoklyuchevskite (4.892 bits/atom), itelmenite (4.644 bits/atom), the previously studied euchlorine (4.440 bits/atom) (Siidra et al., 2019a) (Figures 6,7) and saranchinaite (5.700 bits/atom) (Siidra et al. 2018) are much more structurally complex than the products of their hydration. Despite the decrease in the structural complexity for the complex anhydrous sulfates during hydration, with subsequent heating and dehydration, the complexity increases again and reaches almost its initial values. It is worth noting that the rock-forming minerals of the scoria (Fedotov and Markhinin, 1983) are structurally simple (labradorite 3.700 bits/atom, diopside 2.522 bits/atom, olivine 2.522 bits/atom, chromite 1.379 bits/atom).

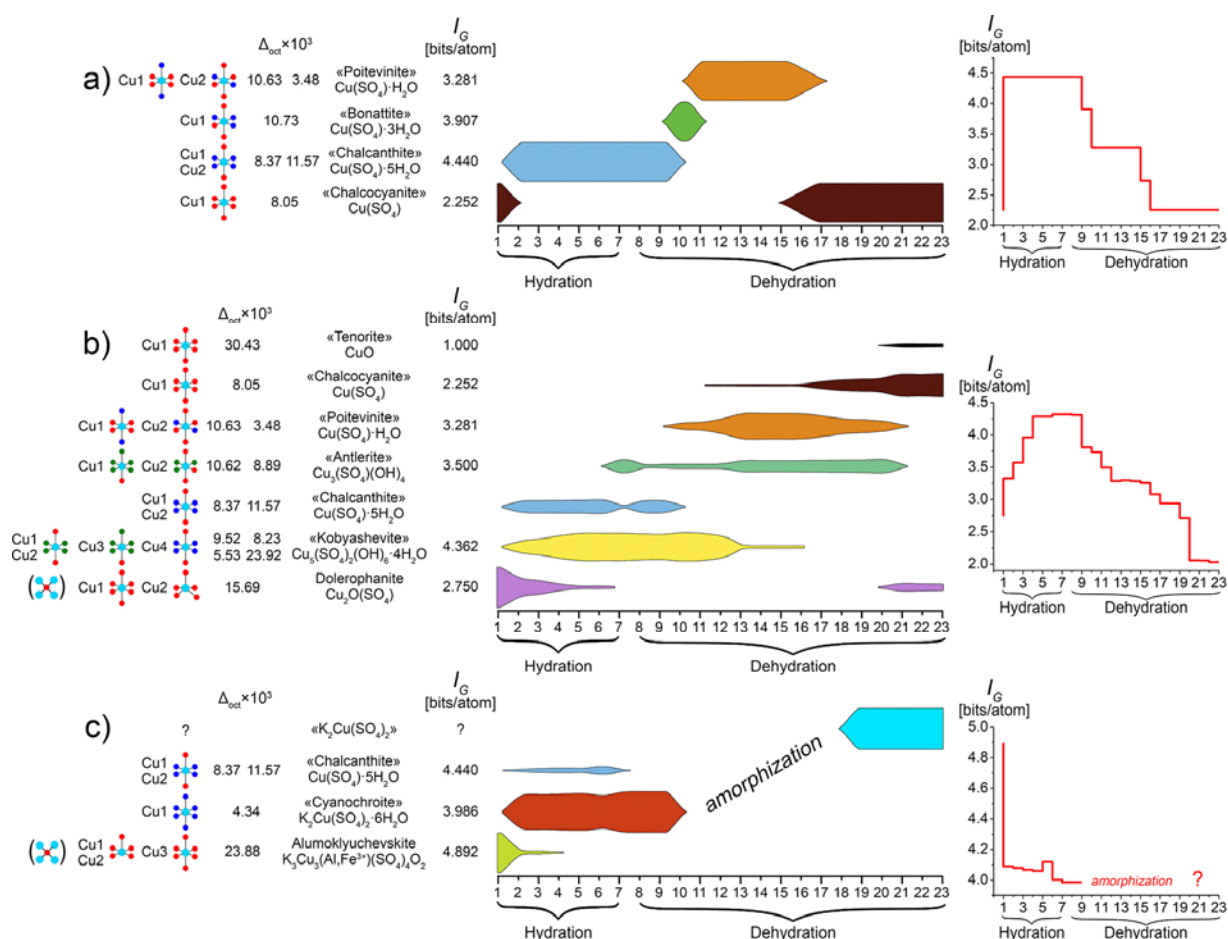


Figure 6. General schemes of the evolution of chalcocyanite (a), dolerophanite (b) and alumoklyuchevskite (c) during the different stages of hydration and dehydration. Evolution of the structural complexity (weighted average values of I_G bits/atom) is shown on the right hand side. I_G bits/atom and types of $\text{CuO}_x(\text{H}_2\text{O})_n(\text{OH})_m$ polyhedra (Cu^{2+} = light blue, O^{2-} = red, H_2O = blue, OH^- = green) in the structure for each mineral phase are shown to the left. $\times 10^3$ bond-length distortion parameter for each Cu-centered octahedron is given.

Changes in coordination of Cu^{2+} cations as a result of hydration/dehydration processes also demonstrate a number of interesting patterns. The types of coordination polyhedra of copper in the structure of each of the minerals or mineral phases, identified during the experiments, are sketched on the left side of Figures 6, 7. All of the Cu-O bonds $< 3\text{\AA}$ were taken into consideration. For the considered anhydrous copper sulfate minerals (and, in general, for other known fumarolic copper sulfates), the following coordination environments are characteristic: square pyramid CuO_5 with different degree of distortion and octahedron CuO_6 . A typical structural characteristic of several anhydrous copper sulfate minerals of fumarolic origin (dolerophanite, euchlorine, alumoklyuchevskite, wulfite), is the presence of oxocentered OCu_4 tetrahedra. These are absent in the structures of all known hydrated minerals or synthetic compounds of the class under consideration. During the transformation to hydrated species (the diversity of which is much greater than that of anhydrous sulfates), a general pattern manifests itself – this is the formation of $[4+2] \text{CuO}_n(\text{H}_2\text{O})_m(\text{OH})_k$ octahedra (Table 7) with different degree of distortion (Figures 6, 7) due

to Jahn-Teller effect. A few exceptions from the [4+2] coordination environments and formation of a [4+1+1] coordination are found in the cases of itelmenite and wulffite. CuO_4OO [4+1+1] strongly distorted polyhedra are observed in both minerals. The coordination environment of Cu^{2+} cations is represented by the three types of ligands, *viz.* O atoms, OH groups, and H_2O molecules. The following Δ_{oct} bond-length distortion parameter, suggested in Wildner (1992), was used for octahedrally coordinated *M* sites in all mineral phases listed in Figures 6,7: where $d_i = (\text{Cu-O})$ bond-length, $d_m = \langle \text{Cu-O} \rangle$ bond-length. As can be seen, the values of $\times 10^3$ are higher for non-protonated CuO_6 octahedra in anhydrous sulfate structures, while for octahedra with the presence of OH groups and H_2O molecules in the coordination of the Cu^{2+} cation, the values are lower. An exception is the $\text{Cu}_4(\text{H}_2\text{O})_4\text{O}_2$ octahedron in the kobyashevite structure, showing the distortion value $\times 10^3 = 23.92$. Conversely, the CuO_6 octahedron in the structure of chalcocyanite has a low $\times 10^3$ value of 8.25, which is not typical for the structures of anhydrous copper sulfates. If we exclude these two octahedra from the calculation, then the average $\langle \times 10^3 \rangle$ for the protonated octahedra in the structures of the considered mineral phases is 8.01, while for anhydrous it is several times higher - 25.19.

Table 7. Minimum, maximum and average equatorial and apical Cu-O bond-length values in $\text{CuO}_x(\text{H}_2\text{O})_n(\text{OH})_m$ octahedra in the structures of mineral phases listed in Figure 6,7 and Table S1, S2.

Anhydrous species				Hydrated species											
Cu-O _{eq}		Cu-O _{ap}		Cu-O _{eq}		Cu-O _{ap}		Cu-OH _{eq}		Cu-OH _{ap}		Cu-H ₂ O _{eq}		Cu-H ₂ O _{ap}	
Cu-O _{eq} min	1.882	Cu-O _{ap} min	2.153	Cu-O _{eq} min	1.942	Cu-O _{ap} min	2.293	Cu-OH _{eq} min	1.907	Cu-OH _{ap} min	2.260	Cu-H ₂ O _{eq} min	1.885	Cu-H ₂ O _{ap} min	2.279
Cu-O _{eq} max	2.070	Cu-O _{ap} max	2.885	Cu-O _{eq} max	2.034	Cu-O _{ap} max	2.660	Cu-OH _{eq} max	2.100	Cu-OH _{ap} max	2.363	Cu-H ₂ O _{eq} max	2.103	Cu-H ₂ O _{ap} max	2.418
$\langle \text{Cu-O}_{eq} \rangle$	1.964	$\langle \text{Cu-O}_{ap} \rangle$	2.623	$\langle \text{Cu-O}_{eq} \rangle$	1.974	$\langle \text{Cu-O}_{ap} \rangle$	2.410	$\langle \text{Cu-OH}_{eq} \rangle$	1.987	$\langle \text{Cu-OH}_{ap} \rangle$	2.305	$\langle \text{Cu-H}_2\text{O}_{eq} \rangle$	1.994	$\langle \text{Cu-H}_2\text{O}_{ap} \rangle$	2.341

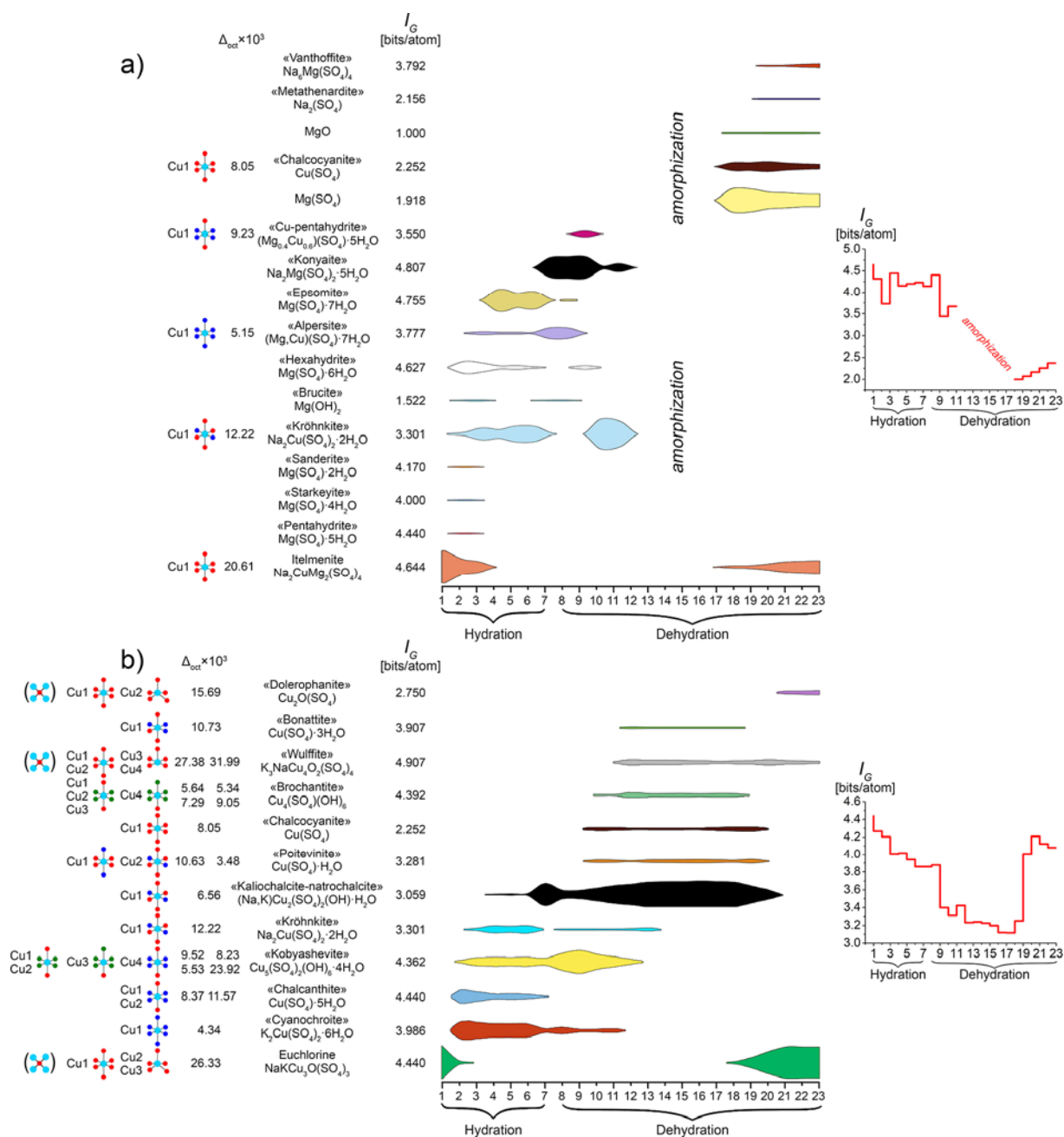


Figure 7. General schemes of the evolution of itelmenite(a) and euchlorine (after Siidra et al., 2019a) (b) during the different stages of hydration and dehydration. Evolution of the structural complexity (weighted average values of I_G bits/atom) is shown to the right. I_G bits/atom and types of $\text{CuO}_x(\text{H}_2\text{O})_n(\text{OH})_m$ polyhedra (Cu^{2+} = light blue, O^{2-} = red, H_2O = blue, OH^- = green) in the structure for each mineral phase are shown to the left. $\times 10^3$ bond-length distortion parameter for each Cu-centered octahedron is given.

The crystal chemistry of divalent copper cations in oxysalts is determined by the Jahn-Teller effect and responsible for the variety of structures and transformation processes during hydration processes. The pronounced Jahn – Teller effect and low crystal field stabilization energy for the $3d^9$ configuration make the coordination sphere of Cu^{2+} particularly non-rigid which enhances these transformations and contributes to structural diversity. Copper polyhedra shown in Figures 6 and 7 show that during the hydration processes, protonated oxygen atoms generally

occupy the equatorial plane, while the apical atoms remain involved in the bonding with sulfate tetrahedra.

Another interesting observation is the pattern of the significantly more complex behavior of fumarolic minerals, as exemplified by dolerophanite, with additional oxygen atoms in its composition (Krivovichev et al., 2013). Overall, the crystal chemistry of hydroxysalts is essentially richer due to greater variability of polymeric M–OH architectures since negatively charged hydroxyl groups can bridge several M cations which is uncommon for neutral water ligands. Therefore, hydration of minerals initially containing O²⁻ anions as parts of oxocomplexes (euchlorine and dolerophanite), proceeds with sequential formation of a large series of hydroxysalts. Formation of several successive hydrated hydroxysalts reflects an evident competition between charged hydroxyl and neutral but more abundant water molecules as ligands. The family of basic copper sulfates, anhydrous and hydrated, is relatively rich; our results, as compared to reference data, indicate that their interconversions are far from being studied in detail. This suggests that, on the one hand, this family will very likely be enriched upon further experimental studies; on the other hand, some more basic copper sulfates, known as synthetic species only, may as likely occasionally be found in nature, particularly if sampling is deliberately performed in “wet” seasons.

On the contrary, hydration of itelmenite with a relatively complex “initial” structure without additional oxygen atoms, which are strong Lewis bases, results in formation of simpler hydrates. The lower the temperature and the larger excess of water, the higher hydration numbers are observed for cations. Ultimately, the more abundant water molecules expel the bridging sulfate anions from the metal coordination sphere yielding relatively simple fully hydrated structures.

Concluding remarks

A study of the evolution of sulfates in hydration and dehydration processes has demonstrated the complexity of the processes for a number of minerals. The temperature regime on the active fumaroles of the scoria cones of the Tolbachik volcano is not constant and changes even over relatively short periods of time, which leads to the formation of large amounts of hydrated minerals in the case of lowering the temperature, and, conversely, in the case of an increase in reversible dehydration for a number of minerals, as shown by us in a number of experiments. It is known that structurally and chemically complex hydroxysalt minerals with various metals, as a rule, are formed as a result of secondary geological processes, such as oxidation zones, crystallization from aqueous solutions, *etc.*, i.e. the presence of water in the systems is responsible for the occurrence of complex structural architectures. These complex

minerals almost invariably contain water or hydroxyl groups. In respect to complexity, fumarolic anhydrous copper minerals with sulfate anions, and especially those containing additional oxygen atoms, form a separate group of primary minerals which reflect both the general complexity of the structures and the complexity of the transformation processes. Moreover, some of the structurally complex anhydrous copper sulfates (euchlorine, alumoklyuchevskite and saranchinaite) can be considered not as rare fumarolic accessory minerals, but rather as rock-forming in primary exhalative mineral assemblages. It is worth noting that H₂O is the main component of gases and an agent for the transport of transition metals in post-eruptive processes on the scoria cones of the Tolbachik volcano (Fedotov and Markhinin, 1983). Above some temperature limit, water is supposed to act mostly as a chemical transporting agent; if the deposition temperature is relatively high, one can expect formation of anhydrous species. Below this limit, formation of hydrated species becomes possible. At temperatures close to ambient, it would be difficult if ever possible to discriminate the effects of exhaled (“intrinsic”) and atmospheric (“extrinsic”) water.

Acknowledgements

This work was financially supported by the Russian Science Foundation through the grant 16-17-10085. Technical support by the SPbSU X-ray Diffraction and Geomodel Resource Centers is gratefully acknowledged. O.I.S. was supported by the internal SPbSU travel grant to the University of Kiel.

References

1. Altheide T., Chevrier V., Nicholson C. and Denson J. (2009) Experimental investigation of the stability and evaporation of sulfate and chloride brines on Mars. *Earth and Planetary Science Letters*, **282**, 69-78.
2. Bacon G.E. and Titterton D.H. (1975) Neutron-diffraction studies of CuSO₄·5(H₂O) and CuSO₄·5(D₂O). *Zeitschrift für Kristallographie*, **141**, 330-341.
3. Balassone G., Petti C., Mondillo N., Panikorovskii T.L., de Gennaro R., Cappelletti P., Altomare A., Corriero N., Cangiano M. and D’Orazio L. (2019) Copper minerals at Vesuvius volcano (Southern Italy): a mineralogical review. *Minerals*, **9**, 730.
4. Baur W.H. (1962) Zur Kristallchemie der Salzhydrate. Die Kristallstrukturen von MgSO₄·4(H₂O) (Leonhardtite) und FeSO₄·4(H₂O) (Rozenite). *Acta Crystallographica*, **15**, 815-826.

5. Baur W.H. and Rolin J.L. (1972) Salt hydrates. IX. The comparison of the crystal structure of magnesium sulfate pentahydrate with copper sulfate pentahydrate and magnesium chromate pentahydrate. *Acta Crystallographica*, **B28**, 1448-1455.
6. Bosi F., Belardi G. and Ballirano P. (2009) Structural features in Tutton's salts $K_2[M^{2+}(H_2O)_6](SO_4)_2$, with $M^{2+} = Mg, Fe, Co, Ni, Cu,$ and Zn . *American Mineralogist*, **94**, 74-82.
7. Brese N.E., O'Keeffe M., Ramakrishna B.L. and Von Dreele R.B. (1990) Low-temperature structures of CuO and AgO and their relationships to those of MgO and PdO. *Journal of Solid State Chemistry*, **89**, 184-190.
8. Bruker. (2014) TOPAS, Version 5.0. Bruker AXS Inc, Madison.
9. Calleri M., Gavetti A., Ivaldi G. and Rubbo M. (1984) Synthetic epsomite, $MgSO_4(H_2O)_7$: absolute configuration and surface features of the complementary $\{111\}$ forms. *Acta Crystallographica*, **B40**, 218-222.
10. Cheng L., Li W., Li Y., Yang Y., Li Y., Cheng Y. and Song D. (2019) Thermal analysis and decomposition kinetics of the dehydration of copper sulfate pentahydrate. *Journal of Thermal Analysis and Calorimetry*, **135**, 2697-2703.
11. Chipera S.J. and Vaniman D.T. (2007) Experimental stability of magnesium sulfate hydrates that may be present on Mars. *Geochimica et Cosmochimica Acta*, **71**, 241-250.
12. Effenberger H. (1985) $Cu_2O(SO_4)$, Dolerophanite: refinement of the crystal structure with a comparison of $[OCu(II)_4]$ tetrahedra in inorganic compounds. *Monatshefte für Chemie*, **116**, 927-931.
13. Fan X.-F., Sun H.-D., Shen Z.-X., Kuo J.-L. and Lu Y.-M. (2008) A first-principle analysis on the phase stabilities, chemical bonds and band gaps of wurtzite structure $A_xZn_{1-x}O$ alloys ($A = Ca, Cd, Mg$). *Journal of Physics: Condensed Matter*, **20**, 235221.
14. Fedotov S.A. and Markhinin Y.K. (editors) (1983) *The Great Tolbachik Fissure Eruption*. Cambridge University Press, New York.
15. Fischer W. and Hellner E. (1964) Ueber die Struktur des Vanthoffits. *Acta Crystallographica*, **17**, 1613-1613.
16. Giester G., Lengauer C. L. and Redhammer G. (1994) Characterization of the $FeSO_4 \cdot H_2O - CuSO_4 \cdot H_2O$ solid-solution series, and the nature of poitevinite, $(Cu,Fe)SO_4 \cdot H_2O$. *The Canadian Mineralogist*, **32**, 873-884.
17. Gorskaya M.G., Vergasova L.P., Filatov S.K., Rolich D.V. and Ananiev V.V. (1995) Alumoklyuchevskite, $K_3Cu_3AlO_2(SO_4)_4$, a new oxysulfate of K, Cu, and Al from volcanic exhalations, Kamchatka, Russia. *Zapiski Rossiiskogo Mineralogicheskogo Obshchestva*, **124**, 95-100.

18. Grevel K.-D. and Majzlan J. (2009) Internally consistent thermodynamic data for magnesium sulfate hydrates. *Geochimica et Cosmochimica Acta*, **73**, 6805-6815.
19. Hawthorne F.C. and Ferguson R.B. (1975) Refinement of the crystal structure of kröhnkite. *Acta Crystallographica*, **B31**, 1753-1755.
20. Hawthorne F.C., Groat L.A. and Eby R.K. (1989) Antlerite, $\text{Cu}_3\text{SO}_4(\text{OH})_4$, a heteropolyhedral wallpaper structure. *Canadian Mineralogist*, **27**, 205-209.
21. Hazen R.M., Papineau D., Bleeker W., Downs R.T., Ferry J.M., McCoy T.J., Sverjensky D.A. and Yang H. (2008) Mineral evolution. *American Mineralogist*, **93**, 1693–1720.
22. Hughes J.M. and Stoiber R.E. (1985) Vanadium sublimates from the fumaroles of Izalco Volcano, El Salvador. *Journal of Volcanology and Geothermal Research*, **24**, 283–291.
23. Kahler E. (1962) Die Kristallstruktur von Dolerophanit, $\text{Cu}_2\text{O}(\text{SO}_4)$, ein Beispiel fuer 5 Koordiniertes Kupfer. *Naturwissenschaften*, **49**, 298.
24. Krivovichev S.V. (2013) Structural complexity of minerals: information storage and processing in the mineral world. *Mineralogical Magazine*, **77**, 275-326.
25. Krivovichev S.V. (2014) Which inorganic structures are the most complex? *Angewandte Chemie - International Edition*, **53**, 654-661.
26. Krivovichev S.V., Mentré O., Siidra O.I., Colmont M. and Filatov S.K. (2013) Anion-centered tetrahedra in inorganic compounds. *Chemical Reviews*, **113**, 6459–6535.
27. Lander L., Rouse G., Batuk D., Colin C.V., Dalla Corte D.A. and Tarascon J.-M. (2017) Synthesis, structure, and electrochemical properties of K-based sulfates $\text{K}_2\text{M}_2(\text{SO}_4)_3$ with $\text{M} = \text{Fe}$ and Cu . *Inorganic Chemistry*, **56**, 2013-2021.
28. Lindström N., Talreja T., Linnow K., Stahlbuhk A. and Steiger M. (2016) Crystallization behavior of $\text{Na}_2\text{SO}_4 - \text{MgSO}_4$ salt mixtures in sandstone and comparison to single salt behavior. *Applied Geochemistry*, **69**, 50-70.
29. Ma H., Bish D.L., Wang H.W. and Chipera S.J. (2009) Determination of the crystal structure of sanderite, $\text{MgSO}_4 \cdot 2\text{H}_2\text{O}$, by X-ray powder diffraction and the charge flipping method. *American Mineralogist*, **94**, 622-625.
30. Menyailov I.A., Nikitina L.P. and Shapar V.N. (1980) Geochemical features of exhalations of Great Tolbachik Fissure Eruption. Moscow: Nauka (in Russian).
31. Mills S.J., Wilson S.A., Dipple G.M. and Raudsepp M. (2010) The decomposition of konyaite: Importance in CO_2 in mine tailings. *Mineralogical Magazine*, **74**, 903–917.
32. Mitev P.D., Gajewski G. and Hermansson K. (2009) Anharmonic OH vibrations in brucite: small pressure-induced redshift in the range 0 - 22 GPa. *American Mineralogist*, **94**, 1687-1697.

33. Nagase K., Yokobayashi H. and Sone K. (1978) Spectrophotometric and thermoanalytical studies on the dehydration of copper (ii) sulfate and its double salts. *Thermochimica Acta*, **23**, 283-291.
34. Nazarchuk E.V., Siidra O.I., Agakhanov A.A., Lukina E.A., Avdontseva E.Yu. and Karpov G.A. (2018) Itelmenite, $\text{Na}_2\text{CuMg}_2(\text{SO}_4)_4$, a New anhydrous sulfate mineral from the Tolbachik Volcano. *Mineralogical Magazine*, **82**, 1233-1241.
35. Nazarchuk E.V., Siidra O.I., Nekrasova D.O., Shilovskikh V.V., Borisov A.S. and Avdontseva E.Yu. (2020) Glikinite, $\text{Zn}_3\text{O}(\text{SO}_4)_2$, a new anhydrous zinc oxysulfate mineral structurally based on OZn_4 tetrahedra. *Mineralogical Magazine*, **84**, 563-567.
36. Nordstrom D.K. (1982) The effect of sulfate on aluminum concentrations in natural waters: some stability relations in the system $\text{Al}_2\text{O}_3 - \text{H}_2\text{O} - \text{SO}_3$ at 298 K. *Geochimica et Cosmochimica Acta*, **46**, 618-692.
37. Pautov L.A., Mirakov M.A., Siidra O.I., Faiziev A.R., Nazarchuk E.V., Karpenko V.Yu. and Makhmadsharif S. (2020) Falgarite, $\text{K}_4(\text{VO})_3(\text{SO}_4)_5$, a new mineral from sublimates of a natural underground coal fire at the tract of Kukhi-Malik, Fan-Yagnob Coal Deposit, Tajikistan. *Mineralogical Magazine*, **84**, 455-462.
38. Pekov I.V., Koshlyakova N.N., Zubkova N.V., Lykova I.S., Britvin S.N., Yapaskurt V.O., Agakhanov A.A., Shchipalkina N.V., Turchkova A.G. and Sidorov E.G. (2018a) Fumarolic arsenates – a special type of arsenic mineralization. *European Journal of Mineralogy*, **30**, 305–322.
39. Pekov I.V., Zubkova N.V. and Pushcharovsky D.Y. (2018b) Copper minerals from volcanic exhalations – a unique family of natural compounds: crystal-chemical review. *Acta Crystallographica*, **B74**, 502–518.
40. Pekov I.V., Zubkova N.V., Yapaskurt V.O., Belakovskiy D.I., Chukanov N.V., Kasatkin A.V., Kuznetsov A.M. and Pushcharovsky D.Y. (2013) Kobyashevite, $\text{Cu}_5(\text{SO}_4)_2(\text{OH})_6 \cdot 4\text{H}_2\text{O}$, a new devilline-group mineral from the Vishnevye Mountains, South Urals, Russia. *Mineralogy and Petrology*, **107**, 201-210.
41. Ramamurthy P. and Secco E.A. (1970) Studies on metal hydroxy compounds. XII. Thermal analyses, decomposition kinetics, and infrared spectra of copper basic oxysalts. *Canadian Journal of Chemistry*, **48**, 3510-3519.
42. Rasmussen S.E., Jorgensen J.E. and Lundtoft B. (1996) Structures and phase transitions of Na_2SO_4 . *Journal of Applied Crystallography*, **29**, 42-47.
43. Rentzeperis P.J. and Soldatos C.T. (1958) The crystal structure of the anhydrous magnesium sulphate. *Acta Crystallographica*, **11**, 686-688.

44. Siidra O.I., Vergasova L.P., Kretser Y.L., Polekhovsky Y.S., Filatov S.K. and Krivovichev S. V. (2014b) Unique thallium mineralization in the fumaroles of Tolbachik Volcano, Kamchatka peninsula, Russia. II. Karpovite, $\text{Tl}_2\text{VO}(\text{SO}_4)_2(\text{H}_2\text{O})$. *Mineralogical Magazine*, **78**, 1699–1709.
45. Siidra O.I., Vergasova L.P., Kretser Y.L., Polekhovsky Y.S., Filatov S.K. and Krivovichev S.V. (2014c) Unique thallium mineralization in the fumaroles of Tolbachik Volcano, Kamchatka peninsula, Russia. III. Evdokimovite, $\text{Tl}_4(\text{VO})_3(\text{SO}_4)_5(\text{H}_2\text{O})_5$. *Mineralogical Magazine*, **78**, 1711–1724.
46. Siidra O.I., Vergasova L.P., Krivovichev S.V., Kretser Y.L., Zaitsev A.N. and Filatov S.K. (2014a) Unique thallium mineralization in the fumaroles of Tolbachik Volcano, Kamchatka peninsula, Russia. I. Markhininite, $\text{TlBi}(\text{SO}_4)_2$. *Mineralogical Magazine*, **78**, 1687–1698.
47. Siidra O.I., Borisov A.S., Lukina E.A., Depmeier W., Platonova N.V., Colmont M. and Nekrasova D.O. (2019a) Reversible hydration/dehydration and thermal expansion of euchlorine, ideally $\text{KNaCu}_3\text{O}(\text{SO}_4)_3$. *Physics and Chemistry of Minerals*, **46**, 403–416.
48. Siidra O.I., Lukina E.A., Nazarchuk E.V., Depmeier W., Bubnova R.S., Agakhanov A.A., Avdontseva E.Yu., Filatov S.K. and Kovrugin V.M. (2018a) Saranchinaite, $\text{Na}_2\text{Cu}(\text{SO}_4)_2$, a new exhalative mineral from Tolbachik Volcano, Kamchatka, Russia, and a product of the reversible dehydration of kröhnkite, $\text{Na}_2\text{Cu}(\text{SO}_4)_2(\text{H}_2\text{O})_2$. *Mineralogical Magazine*, **82**, 257–274.
49. Siidra O.I., Nazarchuk E.V., Agakhanov A.A., Lukina E.A., Zaitsev A.N., Turner R., Filatov S.K., Pekov I.V., Karpov G.A. and Yapaskurt V.O. (2018b) Hermannjahnite, $\text{CuZn}(\text{SO}_4)_2$, a new mineral with chalcocyanite derivative structure from the Naboko Scoria Cone of the 2012–2013 Fissure Eruption at Tolbachik Volcano, Kamchatka, Russia. *Mineralogy and Petrology*, **112**, 123–134.
50. Siidra O.I., Nazarchuk E.V., Lukina E.A., Zaitsev A.N. and Shilovskikh V.V. (2018c) Belousovite, $\text{KZn}(\text{SO}_4)\text{Cl}$, a new sulphate mineral from the Tolbachik Volcano with apophyllite sheet-topology. *Mineralogical Magazine*, **82**, 1079–1088.
51. Siidra O.I., Nazarchuk E.V., Zaitsev A.N. and Shilovskikh V.V. (2020a) Majzlanite, $\text{K}_2\text{Na}(\text{ZnNa})\text{Ca}(\text{SO}_4)_4$, a new anhydrous sulphate mineral with complex cation substitutions from Tolbachik Volcano. *Mineralogical Magazine*, **84**, 153–158.
52. Siidra O.I., Nazarchuk E.V., Zaitsev A.N. and Vlasenko N.S. (2020b) Koryakite, $\text{NaKMg}_2\text{Al}_2(\text{SO}_4)_6$, a new NASICON-related anhydrous sulphate mineral from Tolbachik Volcano. *Mineralogical Magazine*, **84**, 283–287.

53. Siidra O.I., Nazarchuk E.V., Zaitsev A.N., Lukina E.A., Avdontseva E.Yu., Vergasova L.P., Vlasenko N.S., Filatov S.K., Turner R. and Karpov G.A. (2017) Copper oxosulphates from fumaroles of Tolbachik Volcano: Puninite, $\text{Na}_2\text{Cu}_3\text{O}(\text{SO}_4)_3$ – a new mineral species and structure refinements of kamchatkite and alumoklyuchevskite. *European Journal of Mineralogy*, **29**, 499 – 510.
54. Siidra O.I., Nazarchuk E.V., Agakhanov A.A. and Polekhovsky Yu.S. (2019c) Aleutite $[\text{Cu}_5\text{O}_2](\text{AsO}_4)(\text{VO}_4) \cdot (\text{Cu}_{0.5}\square_{0.5})\text{Cl}$, a new complex salt-inclusion mineral with Cu^{2+} substructure derived from Kagome-net. *Mineralogical Magazine*, **83**, 847-853.
55. Siidra O.I., Nazarchuk E.V., Zaitsev A.N., Polekhovsky Yu.S., Wenzel T. and Spratt J. (2019b) Dokuchaevite, $\text{Cu}_8\text{O}_2(\text{VO}_4)_3\text{Cl}_3$, a new mineral with remarkably diverse Cu^{2+} mixed-ligand coordination environments. *Mineralogical Magazine*, **83**, 749-755.
56. Sklute E.C., Rogers A.D., Gregerson J.C., Jensen H.B., Reeder R.J. and Dyar M.D. (2018) Amorphous salts formed from rapid dehydration of multicomponent chloride and ferric sulfate brines: implications for Mars. *Icarus*, **302**, 285-295.
57. Stanimirova T. and Ivanova K. (2019) Transformation of ktenasite-type minerals to langite, posnjakite, and brochantite under water treatment. *Comptes rendus de l'Academie bulgare des Sciences*, **72**, 768-776.
58. Steiger M., Linnow K., Ehrhardt D. and Rohde M. (2011) Decomposition reactions of magnesium sulfate hydrates and phase equilibria in the $\text{MgSO}_4 - \text{H}_2\text{O}$ and $\text{Na}^+ - \text{Mg}^{2+} - \text{Cl}^- - \text{SO}_4^{2-} - \text{H}_2\text{O}$ systems with implication for Mars. *Geochimica et Cosmochimica Acta*, **75**, 3600-3626.
59. Tanaka H. and Koga N. (1988) Preparation and thermal decomposition of basic copper (II) sulfates. *Thermochimica Acta*, **133**, 221-226.
60. Ting V.P., Henry P.F., Schmidtman M., Wilson C.C. and Weller M.T. (2009) In situ neutron powder diffraction and structure determination in controlled humidities. *Chemical Communications*, 7527–7529.
61. Uzunov I., Klissurski D. and Teocharov L. (1995) Thermal decomposition of basic copper sulfate monohydrate. *Journal of Thermal Analysis*, **44**, 685-696.
62. Vaniman D.T., Bish D.L., Chipera S.J., Fialips C.I., Carey J.W. and Feldman W.G. (2004) Magnesium sulphate salts and the history of Water on Mars. *Nature*, **431**, 663-665.
63. Vergasova L.P. and Filatov S.K. (2012) New mineral species in products of fumarole activity of the Great Tolbachik Fissure Eruption. *Journal of Volcanology and Seismology*, **6**, 281-289.
64. Vergasova L.P. and Filatov S.K. (2016) A study of volcanogenic exhalation mineralization. *Journal of Volcanology and Seismology*, **10**, 71-85.

65. Wildner M. (1992) On the geometry of Co(II)O₆ polyhedra in inorganic compounds. *Zeitschrift für Kristallographie*, **202**, 51-70.
66. Xu W., Tosca N.J., McLennan S.M. and Parise J.B. (2009) Humidity-induced phase transitions of ferric sulfate minerals studied by in situ and ex situ X-ray diffraction. *American Mineralogist*, **94**, 1629–1637.
67. Yoder C.H., Agee T.M., Ginion K.E., Hofmann A.E., Ewanichak J.E., Schaeffer C.D.Jr., Carroll M.J., Schaeffer R.W. and McCaffrey P.F. (2007) The relative stabilities of the copper hydroxyl sulfates. *Mineralogical Magazine*, **71**, 571-577.
68. Zahrobsky R.F. and Baur W.H. (1968) On the crystal chemistry of salt hydrates. V. The determination of the crystal structure of CuSO₄·3H₂O (bonattite). *Acta Crystallographica*, **B24**, 508-513.
69. Zalkin A., Ruben H. and Templeton D.H. (1964) The crystal structure and hydrogen bonding of magnesium sulfate hexahydrate. *Acta Crystallographica*, **17**, 235-240.
70. Zhou H.A., Liu Z., Ang S.S. and Zhang J.-J. (2020) Synthesis, structure, and electrochemical performances of a novel three-dimensional framework K₂[Cu(SO₄)₂]. *Solid State Sciences*, **100**, 106104.